Regional structural and functional specializations in the urethra of the female rat : evidence for complex physiological control systems

Regional structural and functional specialisations in the urethra of the female rat: evidence for complex physiological control systems

Authors

Monica Eggermont[1], Stefan De Wachter[1], Jane Eastham[2], James Gillespie[1]

[1] *Department of Urology, Faculty of Medicine and Health Sciences, University of Antwerp, Antwerp, Belgium*

[2] *Uro-physiology Research Group, The Dental and Medical School, Newcastle University, Newcastle upon Tyne, UK*

Corresponding author

Monica Eggermont, M.Sc.

Campus Drie Eiken; T4.93

Universiteitsplein 1

2610 Wilrijk

Belgium

Tel: 003232652535

Fax: 003238214479

Mail: monica.eggermont@uantwerpen.be

Running title: Morphology of the female rat urethra

Conflict of interest: The authors declare that they have no conflict of interest.

Ethical approval: All applicable international, national, and/or institutional guidelines for the care and use of animals were followed.
All procedures performed in studies involving animals were in accordance with the ethical standards of the institution or practice at which the studies were conducted (EC2014-89).

Grant sponsor: no grand sponsors

ABSTRACT

The present study characterises the complex structural and functional elements of the female rat urethra that may be involved in controlling urethral closure and continence. Urethras were dissected from female Sprague-Dawley rats (n=12) euthanized by pentobarbital overdose. Tissues were fixed (4% paraformaldehyde), frozen and sectioned (8μm) for light microscopy and immunohistochemistry. Antibodies were used to detect immunoreactivity to calcitonin gene related peptide, nitric oxide synthase, vesicular acetylcholine transporter and tyrosine hydroxylase. Measurements of urethral wall compliance were taken along its length and in different axes using a closed ended catheter with a circular aperture. The bladder neck and proximal urethra are characterized by a highly folded epithelium and lamina propria. A smooth muscle layer is apparent but not pronounced. Distal to this region the smooth muscle layer thickens and forms the body of the internal sphincter, which has a complex innervation. In the mid urethra the smooth muscle is thickened resulting in a luminal protrusion, producing an occlusion of the lumen. The structure of the distal urethra is different. The epithelium has few folds and, immediately below the lamina propria large thin walled vascular lacunae can be found. Measurements of the urethral wall compliance demonstrate distinct regional differences with proximal and distal specialisations. These variations, which correlate with muscular and vascular elements, suggests the operation of discrete systems, hence effecting urethral closure during filling. An understanding of these systems may yield insights into urethral pathology and direct approaches to develop pharmacological interventions to promote continence.

Key words: rat, urethra, immunohistochemistry, immunofluorescence, compliance profile, morphology

INTRODUCTION

During the storage and voiding phases of the micturition cycle the bladder and its outlet, the urethra, operate as a functional coordinated unit. This coordination is brought about by complex neural control systems that incorporate up to 7 reflex arcs between the bladder-urethra, urethra-bladder, bladder-bladder and urethra-urethra that pass through spinal and supra-spinal pathways (Barrington, 1925, 1931, 1941; Garry et al, 1959).

It is now becoming clear that the afferent outflow from the bladder, the 'afferent noise' is complex involving several functional sensory systems (Gillespie et al., 2009; Kanai and Andersson, 2010) and possibly reflex arcs that involve the peripheral ganglia (Eastham and Gillespie, 2013; Gillespie et al., 2006). Furthermore, different forms of motor activity are also becoming apparent in the bladder wall that are controlled by distinct efferent mechanisms and which may have complex physiological roles (Gillespie et al., 2015a, b). It is remarkable that less is known about the afferent outflow from the urethra and its efferent systems.

In general, the afferent pathways from the lower urinary tract, identified electro-physiologically, are believed to involve small myelinated fibres (Aδ-fibres) and unmyelinated fibres (C-fibres) running in the peripheral nerves innervating the lower urinary tract (LUT): the hypogastric, pelvic and pudendal nerves (de Groat, 2006). There is also evidence suggesting the existence of large myelinated (Aα/β fibres) afferents in the pudendal nerve that innervate the distal urethra (Yoshimura et al., 2003). Recently, urethral afferent fibres associated with fast and slowly adapting receptors have been described in the proximal and distal urethra of the rat (Eggermont et al., 2015). However, the precise micro-anatomical location and subtype classification of these afferents nerves, e.g. as cholinergic, adrenergic, nitrergic or peptidergic, remains to be established.

The mechanisms involved in the efferent reflexes of the urethra are poorly understood. Roles for an internal smooth muscle sphincter and external somatic sphincter have been described in terms of continence mechanisms to maintain closure of the urethra during bladder filling (Zhang et al., 2015). The activation of the external striated sphincter appears to involve cholinergic motor end plates (de Groat et al., 2001). However, the control of the internal sphincter is less well understood and appears to be complex involving adrenergic, cholinergic and peptidergic input (Canda et al., 2008). How these mechanisms integrate with the reflexes described by Barrington are poorly understood (Barrington, 1925, 1931, 1941).

There are indications in the literature that the efferent mechanisms in the urethra are even more complex. In particular these reports relate to a vascular component involved in maintaining urethral closure during filling (Augsburger and Muller, 2000; Bump et al., 1988; Raz et al., 1972; Rud et al., 1980). Here, it has been suggested that the urethral wall has an increased blood flow as the bladder fills and that this engorgement facilitates closure of the urethral lumen (Andersson et al., 1985; Brading et al., 1999). However, the structures involved in this mechanism, their control and precise role in the maintenance of continence are poorly understood.

The purpose of the present study was to undertake a re-evaluation and characterization of the structural elements, afferent and efferent, in the urethral wall. In addition, attempts have been made to begin to explore the functional manifestations of these structural elements.

MATERIALS AND METHODS

Tissue extraction and preparation

A total of 12 female Sprague Dawley rats weighing 200 to 250gm were used. They were maintained under standard laboratory conditions with a 12:12-hour light/dark cycle with free access to food and water. The protocol was approved by the animal ethics committee of the Faculty of Medicine and Health Sciences, University of Antwerp (EC2014-89).

The rats were anesthetized with pentobarbital (60mg/kg, intraperitoneal). The urethra and bladder of each rat was dissected out as a single unit. After dissection, the rats were killed by pentobarbital overdose (3x anaesthetic dose).

Tissue preparation for immunohistochemistry was as previously described (Eastham et al., 2015). Briefly, the urethra and bladder units were removed and pinned onto a Sylgard dish after which the urethras were dissected free at the level of the bladder neck. Tissues were immediately immersion-fixed in 4% paraformaldehyde in phosphate buffer saline (PBS) for 120 min at 4°C. The urethras were then washed in PBS and incubated in solutions with progressively higher sucrose solutions (10, 20 and 30%) to act as a cryo-protectant. Tissues were subsequently 'snap frozen' using isopentane cooled to freezing point with liquid nitrogen. Frozen tissue was then kept at -80°C until needed. Tissue sections (7-8μm) were cut at -25°C and subsequently placed on polysine-coated slides. Four urethras were cut longitudinally and 8 were cut transversely. Tissue morphology was examined using a light microscope to confirm that gross structural features were intact. Of the urethras cut longitudinally, sections were also processed with H&E staining to define the overall cyto-architecture.

Staining procedures

Slides were removed from the freezer and maintained in a dry environment for 120 min at room temperature. They were then washed in tris-buffer saline (TBS), tris-buffer saline tween (TBS-T) and TBS wash cycle for 5 min at each stage. Primary antibodies were diluted with 1x PBS or PBS with triton-X (1%), pH 7.4. Combinations of primary antibodies (1°Abs) were then put on each slide and incubated overnight at 4°C in a humidified chamber.

Primary polyclonal antibodies included against calcitonin gene-related peptide (cgrp) (1:500; Santa Cruz, Cat No. sc-57053), neuronal nitric oxide synthase (nNos) (1:500; Santa Cruz, Cat No. sc-648), tyrosine hydroxylase (TH) (1:5000; Santa Cruz, Cat No. sc-14007), 5-HT (1:200, GeneTex, Cat No. GTX31099) and vesicular acetylcholine transporter (vacht) (1:1000; Sigma, Cat No. V5387). These antibodies were chosen since they have been characterized at the molecular level and previously used in papers (Hoffman et al., 2011; Paille et al., 2010; Peunova et al., 2001).

After overnight incubation, sections were washed in TBS, TBS-T, TBS wash cycles each for 20 mins. Sections were then incubated with appropriate secondary fluorescent antibodies: mouse, goat and rabbit primary antibodies were visualized using donkey anti-mouse/goat/rabbit IgG antibody conjugate (Molecular Probes) Alexa Fluor 488 or 594. Secondary Abs were applied in PBS and used at 1:500 dilutions. The secondary antibodies were applied sequentially and were applied for 1 h at room temperature in a humidified chamber, in a dark environment. After each incubation, slides were washed three times in TBS, TBS-T and TBS. After the final wash, sections were covered with Vectashield hard-set mounting medium with DAPI (nucleic acid molecular probe stain) and over-laid with a coverslip (24x60 mm). Varnish was applied to the coverslip to preserve slides.

Image and microscope analysis

Sections were viewed using an Olympus BX61 fluorescence microscope with x10, x20 and x60 objectives. Images were captured using an Olympus XM10 monochrome camera in 16-bits digital format and further analysed using Image J software (Java-based image processing program, National Institutes of Health (US)).

Urethral compliance measurements

Six female Sprague-Dawley rats (200-250g) were anesthetized with urethane (1,5g/kg IP). They were maintained under standard laboratory conditions with a 12:12-hour light/dark cycle with free access to food and water. The protocol was approved by the animal ethics committee of the Faculty of Medicine and Health Sciences, University of Antwerp (EC2016-40). After the experiments, the rats were killed by urethane overdose (3x anaesthetic dose).

Urethral compliance measurements were obtained in these anesthized rats in prone position using a modified water-perfusion one-hole catheter (2F) system. Saline was infused into the perfusion catheter (0.3ml/min) while the catheter was pulled back through the urethra (1cm/min). The pressure profiles were studied with the aperture oriented towards different surfaces of the urethra (dorsal, ventral, lateral). Control pressure records were compared to sham-operated and bilateral pudendal transection.

The approach used was adapted from the method described by Xu et al., (2015) to measure urethral pressure profiles. However, it is argued here that the method actually measures the compliance of the wall rather than the intrinsic pressure generated within the wall. Briefly, urethral wall signal (compliance) is determined using a closed ended catheter (diameter 0.67 mm) in which an aperture (diameter 0.2 mm) is made 6 mm from the tip. Saline at room temperature was infused into the

perfusion catheter (0.3ml/min), resulting in a basal catheter pressure, while the catheter was pulled back (1cm/min) from the bladder neck to the urethral meatus, giving an estimation of urethral wall compliance along its length in the urethra (see Fig. 8 for a further elaboration of the experimental principle). The catheter aperture was positioned to face the dorsal, ventral and lateral walls of the urethra. Thus, measurements of urethral compliance were made along the urethral length and in different axial directions.

RESULTS

Figures 1 A and B show respectively examples of longitudinal and transverse sections of the urethra. Similar morphological elements were seen in all urethras examined (n=12). In longitudinal sections of the proximal urethra and mid urethra (Fig. 1 A), as described, an outer circular striated muscle layer (ss) was seen to surround a smooth muscle layer (sm). The bladder neck and proximal urethra are characterised by a high degree of epithelial folding (f) (see also below). This prominent feature has not been fully described before. In the distal urethra, the major structural elements were different (Fig. 1 A (b)): there was little or no smooth muscle adjacent to the epithelium and lamina propria but there was a pronounced vascular plexus (bv). These large vessels were thin walled and had the appearance of dilated veins or cavernosae. A smooth muscle layer was found to surround the vascular plexus. These regional differences in smooth muscle distribution, epithelia folding and vascular plexus are also seen in transverse sections (Fig. 1 B). Two additional features can be seen in these transverse sections. In the bladder neck, at the urethrovesical junction (Fig. 1 B (a)) a vascular plexus (bv) can be seen outside the smooth muscle layer. Also, in the mid urethra (Fig. 1 B (c)) the

smooth muscle layer (sm) can be seen to form a distinct bulge that protrudes into the urethral lumen. This feature can also be seen in Figures 4 and 5.

The relationship between the region of epithelial folding and the smooth muscle layer of the bladder neck and proximal urethra is examined in more detail in Figure 2. Figure 2 A shows the region of epithelial folding, illustrating the presence and distribution of cgrp-IR and vacht-IR nerves, at the level of the bladder neck and proximal urethra. For clarity, tracings were made of the epithelial and the muscle layers (lower panel). This region, with a length of 5 mm, was divided into 500 □m sub-regions illustrated by the vertical lines. In each sub-region the total length of epithelium and thickness of the smooth muscle cell layer were measured (Fig. 2 B). This example shows what was seen in all urethra, that the region of thickest smooth muscle is always distal to the region of maximal folding.

A further feature of the smooth muscle in this region was a variation in the distribution of cgrp-IR putative afferent nerves. This is shown in Figure 3. A and B illustrate sections stained for TH (putative motor) and cgrp (putative sensory) from the bladder neck (A) and proximal urethra (B). These regions are identified as 2 and 4 in panel C. The immunohistochemical images show clear TH-IR nerves in the bladder neck and proximal urethra. However, there are fewer cgrp-IR nerves in the muscle of the proximal urethra compared to the bladder neck. This loss of cgrp-IR nerves was quantified by measuring the number of cgrp-IR nerves in identified regions along the bladder neck and urethra. Clearly, there is a progressive loss of afferent nerves in the smooth muscle along the urethra.

Figure 4 A illustrates images of transverse sections of the bladder base, proximal urethra and the mid urethra, which gradually decreased in size (Fig. 4 B). A large oval lumen could be identified at the level of the bladder base while in the proximal urethra the lumen has extensive epithelial folding. In the mid urethra the lumen is crescent-shaped due to the presence of the smooth muscle protrusion

(see also Fig. 1 B (c)). This bulk of smooth muscle was located on the dorsal side in all urethras. The characteristics of this muscle protrusion are explored in Figure 5 in sections stained with antibodies to TH, vacht and cgrp. A dense innervation of TH-IR and vacht-IR fibres suggests a complex dual motor innervation. The presence of a distinct but sparse cgrp-IR suggests the presence of some sensory outflow. Panel A shows transverse sections while B longitudinal sections. In A the nerves appear as short 'dot like' structures while in B the structures appear as distinct fibres. This implies that the fibres run predominantly in a longitudinal orientation.

The most dramatic morphological differences between the proximal and distal urethra is the presence of a distinct vascular plexus lying immediately below the epithelium in the distal urethra (Fig. 6). The walls of the vascular plexus have a dense innervation primarily of vacht-IR fibres. Figure 7 illustrates, in more detail, the complex and multiple innervation of the large vessels in the distal urethra. The presence of vacht-IR and nNos-IR fibres, and the presence of cgrp-IR fibres respectively suggest a dual efferent and afferent innervation of these vessels.

In an attempt to determine whether this complex pattern of structural elements could be correlated with any functional characteristics, measurements of urethral wall compliance were made along its length (see Xu et al., (2015) and legend Fig. 8). Typical pressure profiles with the aperture directed at the dorsal, ventral, left and right lateral wall are illustrated in Figure 8 E (b). The 0 mm position is taken to be the first point of increased resistance, assumed to be the urethrovesical junction (UVJ). Based on the structural analysis above, a cartoon illustrating the different structural aspects is also shown (Fig. 8 E (a): see also Fig. 9). At least two broad regional differences could be detected in the compliance profiles: one 2-5 mm from the UVJ and a second 7-10 mm from the UVJ. These two

functional regions appear to correlate with the region of the proximal urethra with smooth muscle and, in the distal urethra, a region of high vascularity. Both regions appear to contribute to the overall occlusion of the urethra.

DISCUSSION

Despite the extensive use of rats in studies of the lower urinary tract there are only a limited number of studies that have described in detail the morphology and anatomy of the female rat urethra (Kim et al., 2007; Lim et al., 2013; Praud et al., 2003; Zhang et al., 2015). Most studies focused on the anatomy and location of the smooth muscle, describing circular and longitudinal smooth layers, and the external striated muscle sphincter surrounding the proximal and mid urethra. The coordinated control of these two independent systems has formed the basis of our understanding of the mechanisms controlling the urethra and producing continence (Bennett et al., 1995; de Groat et al., 2001). The present study has further explored the structural and functional specializations of the female rat urethra. The observations suggest the presence of additional mechanisms that have previously not been fully explored. Given this additional complexity it is now essential to consider the relative importance and contribution of each mechanism to urethral function, lower urinary tract reflexes and the maintenance of continence.

The images presented here show clearly that the bladder neck and the proximal urethra is highly folded. It is likely that these folds occur in the empty bladder. These results imply that, as the bladder fills, the folds may open out to accommodate the increased bladder volume, while the rest of the urethra is still sealed. At which bladder volume this occurs is not known. The observation that the majority of the internal smooth muscle sphincter lies distal to the folded area suggests that this specialization facilitates the unfolding while maintaining urethral closure. Continence is maintained

by the activity in both the internal smooth muscle sphincter and the external sphincter, together with additional factors such as the vascular tissue, elastic tissue and connective tissue (Raz et al., 1972; Rud et al., 1980). Moreover, as noted previously by Gabella et al (Gabella and Davis, 1998) and also in this study, the sub-urothelial layer in this region has a dense innervation of cgrp-IR nerves, which are presumed to be afferent. So, as the bladder fills and pressure rises it is likely that the folds open out (while the urethra is closed), therefore activating the underlying afferent fibres. These afferent fibres could send specific information on the later phases of filling to the central nervous system. It is clear that the majority of the afferent outflow from this region originates from the suburothelial region. It is noteworthy that the cgrp-IR innervation (putative sensory) of the smooth muscle is sparse. This might be interpreted to suggest that for the smooth muscle in this region, there is only a limited afferent outflow and a weaker role for the afferents in the overall coordinated control of the region. The transition from an empty bladder to a full bladder with epithelial unfolding in the presence of proximal urethral contraction is illustrated in Figure 9 A and 9 B (I).

A distinctive and consistent feature of the urethra in this study was the presence of a distinct bulge of smooth muscle located at the dorsal urethral wall of the mid urethra. The consistence of observation and that a similar structure is not seen in other regions of the urethra suggest that this bulge of smooth muscle has a functional specialization. The protrusion contains predominantly smooth muscle and its presence suggests that it might occlude the lumen restricting urine flow and possibly contribute to continence. The nerves and fibres in this region appear to run longitudinally suggesting that contraction would generate the bulge while relaxation would facilitate luminal opening. A region of longitudinal smooth muscle has been described previously towards the dorsal surface in the mid urethra (Lim et al., 2013). It is possible that the bulge described here is an illustration of the same structure. Further, Ulmsten et al (Ulmsten et al, 1977) described a highly

specific adrenergic innervated region of smooth muscle located in the mid urethra of the guinea-pig which correlated with the maximum intraurethral pressure recorded. It is likely that this identified bulge region in the rat is similar to the described adrenergic region in the guinea-pig and therefore has a dominant function in urethral continence. Moreover, in this region distinct TH-IR, vacht-IR and cgrp-IR nerves are found. The precise roles of the fibres with these different immunochemical characteristics are not known. One possibility is that there are at least two efferent control systems, an adrenergic and a cholinergic system as has been described for the proximal urethra (de Groat et al., 2001). The presence of cgrp-IR fibres suggests that this region also has a sensory function. Overall, this mid-urethral mechanism may represent a separate and distinct mechanism contributing to the coordinated control of the urethra. The operation of this region in contributing to luminal opening and closure is also illustrated in Figure 9 B (II).

The structures within the distal urethra are very different. Of particular note is the presence of a distinct vascular plexus lying immediately below the epithelium and lamina propria. These vessels are thin walled and are thus likely to represent a venous plexus. The structure also has the appearance of cavernosal tissue. Critically, in this region, there is no smooth muscle layer adjacent to the lamina propria although a thin layer is found in the outer margins. Also, here, the striated muscle sphincter is less prominent. Thus, closure of the urethral lumen must be derived from an occlusion related to filling of the venous vascular component rather that from the smooth or striated muscle layers. Dilation of the vascular plexus, an engorgement of the wall with blood, would occlude the lumen while a vasoconstriction, draining the venous plexus, would facilitate luminal opening (see Fig. 9 B (III and IIII). Several studies have speculated about the participation of a vascular component in the resting urethral closure mechanism (Augsburger and Muller, 2000; Bump et al., 1988; Raz et al., 1972; Rud et al., 1980). In these studies the blood supply to the whole urethra was occluded, making it difficult to

determine the contribution of any proximal and distal vascular plexus in the resting urethral closure pressure. However, it was suggested that the vascular component of the urethra exceeds the requirements of urethral blood supply and may contribute to one third of the resting tone in the urethra (Rud et al., 1980). Further, it is well know that postmenopausal women are less capable of continence. The lack of estrogen affects the urinary tract and changes the lining of the urethra by diminishing the vascular component (Jarmy-Di Bella et al, 2007). In an experimental study by Zinner et al (Zinner et al, 1980), it was concluded that the ability of the urethral wall to deform, mold and conform was correlated with higher leak point (LPP) pressures. The vascular plexus may play a major role in this urethral wall "softness", thus play a major role in the urethral seal. These data demonstrate a role for blood vessels in determining urethral compliance, possibly along its entire length. In contrast, the data from the rat demonstrate a highly specialized region of vascular cavernosae that contribute to the wall compliance in the distal part of the urethra. Also, these vessels are highly innervated. The detection of vacht-IR, nNos-IR and cgrp-IR nerves in the wall of the vascular structures suggests complex regulation of vessel tone involving cholinergic and nitrergic mechanisms. The presence of cgrp-IR, possible afferent fibres, also raises the possibility that the information relating to the degree or presence of the vasodilatation can be transmitted to the CNS as part of the integrated reflex control of urethral closure. In the present study, in contrast to others, these vessels are particularly prominent. This may be related to the use of barbiturates as an anaesthesia in this study as it is well recognized that barbiturates produce a profound peripheral vasodilatation.

Although a direct role for a urethral vascular plexus in urethral occlusion or during micturition has not yet been demonstrated, it has been shown that urinary flow through the urethra was associated with a mild relaxation of the corporal sinusoids and a mild cavernosus muscle contraction in men. This suggests an 'urethro-corporocavernosal" reflex (Shafik et al., 2008). This reflex was also seen in both

men and women after intra-urethral stimulation of the distal urethra (Shafik et al., 2007). The relation of the corporal sinusoids and contraction of the cavernosus muscle would imply a stretching of the urethra for better passage of urine, making the role of the vascular plexus in continence inferior during micturition after relaxation of the urethral smooth and striated muscle.

One important point to consider is the complex distribution of putative sensory fibres (cgrp-IR) throughout the urethra. Fibres are found in the subepithelial proximal urethra, in the smooth muscle sphincter, the vessel walls of the cavernosal structures and associated with the epithelium of the mid and distal urethra. It is unlikely that all these fibres sense the same modality. Consequently, studies involving single unit afferent recording need to take into account this micro-anatomical complexity.

The present study has identified structural specialisations in different regions of the female rat urethra. What is now critical is to identify and characterise what the functional contribution of each of these elements could be to overall urethral function. In an attempt to begin such a characterization, an approach, previously described in the literature, was used to assess the urethral pressure profile in female rats (Xu et al., 2015). In this original study, a progressive increase in urethral pressure could be identified within the proximal urethra with a peak pressure occurring within the mid urethral segment. The observations described in this paper are in keeping with this observation (see Fig. 8 E) where there is a region of low compliance in the proximal and mid urethra, in the region of maximum internal smooth muscle sphincter thickness and external sphincter thickness. Measurements of compliance also show an additional resistance element in the distal urethra. This region coincides with the region of the vascular plexus. Thus, the vascular component can function as a urethral closure mechanism and so be involved in maintaining continence. Orientation of the catheter aperture in different directions reveals differences in wall compliance in the distal urethra. The reason for this is not known

but may be related to variations in the extent of the vascular network or variations in the supportive connective tissues components.

Next to urethral compliance, it is relevant to note that urethral competence can also be evaluated by the use of an urodynamic parameter, the leak point pressure (LPP). Defined as the bladder pressure at which urine leaks from the urethra in the absence of a detrusor contraction. The LPP has been demonstrated and defined in a variety of rat experiments (Jiang et al, 2011; Cannon and Damaser, 2001). The contribution of different neurological factors and other contributors to continence with the use of LPP measurements has recently been described in female rats (Jiang et al, 2011). Similarly, the present data suggest that several components underline the urethral continence mechanism, which is complex and multifactorial. All these structural components will contribute to the LPP in the female rat.

The structural complexities of the female rat urethra are summarized in Figure 9. In addition, the opening of the bladder neck, to open the folds, and the opening of the closure elements along the urethral length are illustrated: internal smooth muscle sphincter, external striated sphincter, mid urethral smooth muscle thickening and the plexus of distal urethral blood vessels. It seems more than likely that the opening of the folds of the bladder neck and proximal urethra occurs as the bladder fills, reaching a maximum at high bladder volumes. In humans, the bladder neck is seen to dilate immediately prior to voiding (Tanagho and Miller, 1970). Strong sensations of a desire to void are associated with this opening of the bladder neck (Wyndaele and De Wachter, 2008). The same may be true in the rat. Opening of the folds and activation of the afferent fibres may be associated with the arousal behaviours observed in the conscious rat during standard filling cystometry (Streng et al., 2006).

The sequence of events involving either the opening or closing of the urethral elements during the filling or voiding cycle are not known. There may be one sequence during the early stages of a void and a different one to stop or slow urine flow at the end. Also, different elements may play different roles during filling when the stress on the urethra to remain closed changes as bladder pressure increases. Thus, reflex activation of the different control elements may involve a coordinated single reflex or involve multiple and independent reflex mechanisms in the urethra.

The extrapolation of these observations and concepts of regulation to human deserves caution. Although some of the elements are the same their precise anatomical arrangement and functional consequences cannot be assumed. However, a realization that the urethra has such complexities raises questions about the origins of urethral pathologies in the human, stress incontinence, urethral instability and urethra weakness. Since there is possibly different discrete systems operating, this raises the possibilities for specific pharmacological interventions to modulate particular urethral continence related mechanisms.

What is clear is that the urethra is not a simple structure with a simple single function. The complexities identified and discussed clearly demonstrate the need for more detailed studies of integrated urethral function.

LITERATURE CITED

Andersson PO, Bloom SR, Mattiasson A, Uvelius B. 1985. Changes in vascular resistance in the feline urinary bladder in response to bladder filling. J Urol 134:1041-1046.

Augsburger H, Muller U. 2000. Investigation of the female canine urethral vascular plexus using light and scanning electron microscopy: a contributing factor to urinary continence. Cells Tissues Organs 167:239-246.

Barrington FJF. 1925. The effects of lesions of the hind and midbrain on micturition in the cat. J Exper Physiol 15:81-102.

Barrington FJF. 1931. The component reflexes of micturition in the cat. Parts I and II. Brain 54:177-188.

Barrington FJF. 1941. The component reflexes of micturition in the cat. Part III. Brain 64:239–243.

Bennett BC, Kruse MN, Roppolo JR, Flood HD, Fraser M, de Groat WC. 1995. Neural Control of Urethral Outlet Activity in-Vivo - Role of Nitric-Oxide. J Urol 153:2004-2009.

Brading AF, Greenland JE, Mills IW, McMurray G, Symes S. 1999. Blood supply to the bladder during filling. Scand J Urol Nephrol Suppl 201:25-31.

Bump RC, Friedman CI, Copeland WE. 1988. Non-neuromuscular determinants of intraluminal urethral pressure in the female baboon: relative importance of vascular and nonvascular factors. J Urol 139:162-164.

Canda AE, Cinar MG, Turna B, Sahin MO. 2008. Pharmacologic targets on the female urethra. Urol Int 80:341-354.

Cannon TW, Damaser MS. 2001. Effects of anesthesia on cystometry and leak point pressure of the female rat. Life Sci 69:1193-202.

de Groat WC, Fraser MO, Yoshiyama M, Smerin S, Tai C, Chancellor MB, Yoshimura N, Roppolo JR. 2001. Neural control of the urethra. Scand J Urol Nephrol 35:35-43.

de Groat WC. 2006. Integrative control of the lower urinary tract: preclinical perspective. Brit J Pharmacol 147:S25-S40.

Eastham J, Gillespie JI. 2013. The concept of peripheral modulation of bladder sensation. Organogenesis 9:224-233.

Eastham J, Stephenson C, Korstanje K, Gillespie JI. 2015. The expression of beta3-adrenoceptor and muscarinic type 3 receptor immuno-reactivity in the major pelvic ganglion of the rat. Naunyn Schmiedebergs Arch Pharmacol 388:695-708.

Eggermont M, Wyndaele JJ, Gillespie J, De Wachter S. 2015. Response Properties of Urethral Distension Evoked Unifiber Afferent Potentials in the Lower Urinary Tract. J Urol 194:1473-1480.

Gabella G, Davis C. 1998. Distribution of afferent axons in the bladder of rats. J Neurocytol 27:141-155.

Garry RC, Roberts TD, Todd JK. 1959. Reflexes involving the external uretral sphincter in the cat. J Physiol 149:653-665.

Gillespie JI, Markerink-van Ittersum M, de Vente J. 2006. Sensory collaterals, intramural ganglia and motor nerves in the guinea-pig bladder: evidence for intramural neural circuits. Cell Tissue Res 325:33-45.

Gillespie JI, van Koeveringe GA, de Wachter SG, de Vente J. 2009. On the origins of the sensory output from the bladder: the concept of afferent noise. BJU Int 103:1324-1333.

Gillespie JI, Rouget C, Palea S, Granato C, Birder L, Korstanje C. 2015a. The characteristics of intrinsic complex micro-contractile activity in isolated strips of the rat bladder. Naunyn Schmiedebergs Arch Pharmacol 388:709-718.

Gillespie JI, Rouget C, Palea S, Korstanje C. 2015b. The actions of prolonged exposure to cholinergic agonists on isolated bladder strips from the rat. Naunyn Schmiedebergs Arch Pharmacol 388:737-747.

Hoffman EM, Zhang Z, Anderson MB, Schechter R, Miller KE. 2011. Potential Mechanisms for Hypoalgesia Induced by Anti-Nerve Growth Factor Immunoglobulin Are Identified Using Autoimmune Nerve Growth Factor Deprivation. Neuroscience 193:452-465.

Jarmy-Di Bella, ZI, Girao MJ, Di Bella V, Santori MG, Szejnfeld J, Baracat EC, Lima, GR. 2007. Hormonal influence on periurethral vessels in postmenopausal incontinent women using Doppler velocimetry analysis. Maturitas 56:297-302.

Jiang HH, Salcedo LB, Damaser MS. 2011. Quantification of neurological and other contributors to continence in female rats. Brain Res 25:198-205.

Kanai A, Andersson KE. 2010. Bladder afferent signaling: recent findings. J Urol 183: 1288-1295.

Kim RJ, Kerns JM, Liu S, Nagel T, Zaszczurynski P, Lin DL, Damaser MS. 2007. Striated muscle and nerve fascicle distribution in the female rat urethral sphincter. Anat Rec 290:145-154.

Lim SH, Wang TJ, Tseng GF, Lee YF, Huang YS, Chen JR, Cheng CL. 2013. The Distribution of Muscles Fibers and Their Types in the Female Rat Urethra: Cytoarchitecture and Three-Dimensional Reconstruction. Anat Rec 296:1640-1649.

Paille V, Picconi B, Bagetta V, Ghiglieri V, Sgobio C, Di Filippo M, Viscomi MT, Giampa C, Fusco FR, Gardoni F, Bernardi G, Greengard P, Di Luca M, Calabresi P. 2010. Distinct levels of dopamine denervation differentially alter striatal synaptic plasticity and NMDA receptor subunit composition. J Neurosci 30:14182-14193.

Peunova N, Scheinker V, Cline H, Enikolopov G. 2001. Nitric oxide is an essential negative regulator of cell proliferation in Xenopus brain. J Neurosci 21:8809-8818.

Praud C, Sebe P, Mondet F, Sebille A. 2003. The striated urethral sphincter in female rats. Anat Embryol (Berl) 207:169-175.

Raz S, Caine M, Zeigler M. 1972. The vascular component in the production of intraurethral pressure. J Urol 108:93-96.

Rud T, Andersson KE, Asmussen M, Hunting A, Ulmsten U. 1980. Factors maintaining the intraurethral pressure in women. Invest Urol 17:343-347.

Shafik A, Shafik AA, El Sibai O, Shafik IA. 2007. The response of the corporal tissue and cavernosus muscles to urethral stimulation: an effect of penile buffeting of the vaginal introitus. J Androl 28:853-857.

Shafik A, Shafik IA, El Sibai O, Shafik AA. 2008. Study of the response of the penile corporal tissue and cavernosus muscles to micturition. BMC Urol 8:4.

Streng T, Hedlund P, Talo A, Andersson KE, Gillespie JI. 2006. Phasic non-micturition contractions in the bladder of the anaesthetized and awake rat. BJU Int 97:1094-1101.

Tanagho EA, Miller ER. 1970. Initiation of voiding. Br J Urol 42:175-183.

Ulmsten U, Sjöber NO, Alm P, Andersson KE, Owman C, Walles B. 1977. Functional role of an adrenergic sphincter in the female urethra of the guinea-pig. Acta Obstet Gynecol Scand 56:387-390.

Wyndaele JJ, De Wachter S. 2008. The sensory bladder (1): An update on the different sensations described in the lower urinary tract and the physiological mechanisms behind them. Neurourol Urodyn 27:274-278.

Xu S, Li X, Xu L, Chen B, Tan H, Du G. 2015. A Method for Recording Urethral Pressure Profiles in Female Rats. PloS ONE 10:e0140851.

Yoshimura N, Seki S, Erickson KA, Erickson VL, Hancellor MB, de Groat WC. 2003. Histological and electrical properties of rat dorsal root ganglion neurons innervating the lower urinary tract. J Neurosci 23:4355-4361.

Zhang X, Alwaal A, Lin G, Li H, Zaid UB, Wang G, Wang L, Banie L, Ning H, Lin CS, Guo Y, Zhou L, Lue TF. 2015. Urethral musculature and innervation in the female rat. Neurourol Urodyn 35:382-9.

Zinner NR, Sterling AM, Ritter RC. 1980. Role of inner urethral softness in urinary continence. Urology 16:115-7.

FIGURES LEGENDS

D	dorsal
lum	lumen
epi	epithelium
sm	smooth muscle
ss	striated muscle sphincter
det	detrusor
F	epithelial folds
bv	blood vessels
lp	lamina propria
BB	bladder base
BN	bladder neck
PU	proximal urethra
M	muscle mass
f	flow
p	pressure
r	resistance
t	thickening
V	ventral
UVJ	urethrovesical junction
EUM	external urethral meatus

Figure 1 Morphology of different regions of the female rat urethra. Each panel shows sections stained with H and E. [A] shows longitudinal sections of the urethra illustrating (a) the bladder neck and proximal urethra and (b) the mid and distal urethra. [B] shows transverse sections taken from different positions along the urethra; (a), bladder neck (b), proximal urethra (c), mid urethra (d), distal urethra and (e) external urethral meatus. The dorsal aspect of the urethra are marked (D). Individual features are identified: lumen (lum), epithelium (epi), smooth muscle (sm), striated muscle sphincter (ss), detrusor (det), epithelial folds (F) and blood vessels (bv). Scale bars in each panel are 800μm.

Figure 2 Illustration of urethral folding in the bladder neck/proximal urethra and the position of the muscle sphincters. [A] the upper panel is a montage of images illustrating the bladder neck and proximal urethra over a distance of 5 mm (vertical lines are 500 μm apart). It shows immunofluorescent images illustrating staining for cgrp (green), vacht (red) and the nuclear stain dapi (blue). The lumen (lum), epithelium (epi), smooth muscle internal sphincter (sm) and striated muscle sphincter (ss) are indicated. The region of high folding is also shown (F). The lower section is a tracing of the features in the upper panel drawn for clarity, showing the epithelium (solid line) and the internal sphincter (dotted line). [B] illustrates an analysis of this section depicting the total length of epithelium within successive 500 μm wide regions along the urethra (grey histograms). The thickness of the smooth muscle layer is also shown for the corresponding 500 μm intervals along the urethra (o). Note that the point of maximum muscle thickness is distal to the point of maximal urethral folding. Similar data showing such a displacement between the position of maximum folding and maximum smooth muscle thickness were seen in all urethras studied (n=5).

Figure 3 Illustration of the putative sensory innervation of the smooth muscle in the bladder neck and proximal urethra. Smooth muscle is illustrated in the bladder neck [A] and proximal urethra [B]. The sections are stained for the nerve markers TH (red), cgrp (green) and the nuclear marker dapi (blue). The upper panels show the combined images while the middle and lower show the composite TH and cgrp images. The epithelium (epi), lamina propria (lp), smooth muscle (sm) and striated muscle sphincter (ss) are indicated. Regions of the smooth muscle are identified (dotted lines) for nerve profile analysis. Note the near absence of cgrp-IR fibres in the smooth muscle of the proximal urethra. Calibration bars in [A] and [B] are 150 μm. [C] shows a more detailed analysis of the distribution of cgrp-IR fibres. The upper panel identifies 5 arbitrary regions (1-5) in the bladder base (BB), bladder neck (BN) and proximal urethra (PU). Section [A] corresponds with arbitrary region 2 and section [B] corresponds with arbitrary region 4. In each of the arbitrary regions (1-5) the extent of cgrp innervation was determined in representative area by determining fibre length per area. Values are mean $\pm$ standard deviation (n=5) for representative areas. Note the clear reduction in cgrp innervation in the smooth muscle of the proximal urethra.

Figure 4 Cross sections of the bladder base, proximal and mid urethra. [A] illustrates 3 transverse sections stained for the neuronal markers 5HT (green), vacht (red) and the nuclear marker dapi (blue). The left panel shows the large lumen diameter of the bladder base. The middle panel shows the high degree of epithelial folding in the proximal urethra. The right panel illustrates a thickening of the smooth muscle in the mid urethra. Note that, in this region, this is on the dorsal side (D) of the urethra and protrudes into the lumen, coming into close proximity

with the ventral surface. Calibration bars in [A], [B] and [C] are 200 μm. [B] illustrates an analysis of the lumen dimensions at different locations along the urethra. In order to take into account the folding of the urethral wall, measurements were made of the lumen cross-sectional area. Data are mean values ± standard deviation (n=7).

Figure 5 Illustration of the innervation of the luminal protrusion on the dorsal side of the mid urethra. [A] shows low power transverse sections of the thickening in the mid urethra stained (from left to right) for TH (red) and cgrp (green); vacht (red) and cgrp (green); nNos (red) and cgrp (green). All sections are also stained for dapi (blue). The middle panels shows higher resolution images of [A] (boxes) illustrating distinct TH, vacht and nNos-IR nerve fibres as well as cgrp-IR fibres. Note the orientation of the fibres that appears as 'dots' or short structures. [B] shows images from a different urethra illustrating the innervation in the same mid-urethral region with the same stainings. In this preparation the tissue was cut longitudinally. Note that here the fibres appear long suggesting that they run predominantly parallel to the long axis of the tissue. Calibration bars: [A], 200 μm; middle panels, 20 μm; [B], 20 μm.

Figure 6 The distribution of large blood vessels in the proximal and distal urethra. [A] and [B] show respectively transverse H and E sections of the proximal urethra and distal urethra. In each panel examples of vessels are indicated (*). Note that in the proximal urethra the vessels are located primarily between the major muscle mass (M) and the fascia of the dorsal margin (D). In the distal urethra, a region of dense vessels is seen close to the lumen (lum). [C] and [D] show sections of the proximal and distal urethra respectively stained for the nerve markers cgrp (green) and vacht (red). Sections are also stained for the nuclear marker dapi (blue). Note, in the

proximal urethra, the presence of cgrp-IR fibres close to the epithelium (epi) but not in the smooth muscle layer (sm). In the distal urethra, vacht-IR fibres are seen in close proximity to the vessels. Calibration bars: [A]/[B] 800μm and [C]/[D] 200 μm. lp = lamina propria.

Figure 7 High resolution images illustrating the innervation of the blood vessels in the distal urethra. [A] shows a section stained for the nerve markers vacht (red) and cgrp (green). All sections are also stained for the nuclear marker dapi (blue). The left panel shows a low power image while the right panels show the identified regions (boxes) at higher magnification. Vessel lumens are indicated (*). Arrows point to distinct vacht-IR and cgrp-IR fibres in the wall of the vessels. [B] shows sections stained for nNos (red), cgrp (green) and dapi (blue). Vessel lumen are indicated (*) and arrows point to distinct nNos-IR nerves. The panels on the right show the identified regions (boxes) of the image on the left at higher magnification. nNos-IR nerves are clearly seen in the vessel wall. Calibration bars in [A] and [B] large panels are 15 μm and side panels are 6 μm.

Figure 8 Estimation of urethral wall compliance along its length and on different axes [A] illustrates the aperture of the closed ended catheter (catheter diameter 0.67 mm, aperture diameter 0.2 mm). Saline is forced through the opening at a rate of 0.3 ml/min (direction of flow (f) illustrated by arrows) resulting in a basal catheter pressure (p). When the catheter opening is brought close to the urethral wall the resistance to flow (r) increases and the pressure rises. If the urethral wall over the aperture is passive and elastic (high compliance (c)) then the wall will contribute only a small amount to the resistance and the catheter pressure will remain close to basal pressure. However, if the wall is stiff (low compliance), the fluid flow will not displace the

wall and the resistance to flow will be greater. As a result, the pressure in the catheter will rise. The catheter pressure is therefore, in part, related to the compliance of the underlying urethral wall. [B] illustrates a simple representation of the elements of the system. [C] illustrates the catheter with the aperture in the bladder lumen (a) and as it is pulled through the urethra (b). The dotted lines are assumed to represent the urethrovesical junction (UVJ) and the external urethral meatus (EUM). [D] illustrates the position of the aperture in relation to the urethral wall. The aperture can be rotated to estimate the wall compliance in the dorsal and ventral aspects and also in the lateral walls. [E] (b) illustrates 4 sample records of catheter pressure from one animal (supine position) as the catheter is pulled from the bladder through the urethra (10mm/min). The different traces were made with the aperture pointing to the dorsal, ventral, left lateral and right lateral wall. A reference point to identify the position of the aperture was determined by the position of first pressure inflection during a withdrawal (0mm). Negative values represent positions where the aperture is in the bladder and positive values at different positions along the urethra. The cartoon summarizing the morphological features along the urethra is also shown (a) in an attempt to relate structures to the pressure/compliance changes (see legend Fig. 9 for details).

Figure 9 Cartoons summarizing the major structural elements observed in the female rat urethra. [A] shows the major elements: detrusor (det), folded epithelium of the proximal urethra (f), striated muscle sphincter (ss), smooth muscle (sm), mid urethral smooth muscle thickening (t) and distal urethral blood vessels (bv). The bladder neck (BN), the urethra, ventral (V) and distal (D) positions are shown. Panel A also illustrates a possible arrangement where all of the different elements are in place to produce a closed urethra, i.e. as during the filling or

storage phase. [B] illustrates how each of the component systems might change to lead to an opening of the urethral lumen: (I) opening of the bladder neck and unfolding of the proximal epithelial folds, (II)/(III) opening urethral lumen by relaxation of urethral smooth and striated muscle, and (IIII) opening distal urethral lumen by overcoming of vesical resistance.

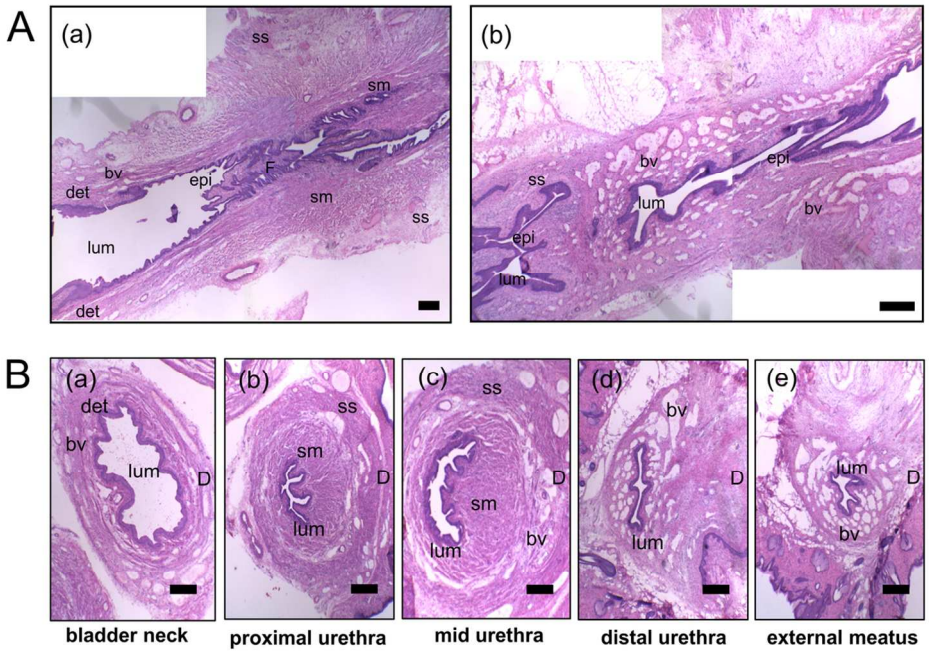

Fig. 1. Morphology of different regions of the female rat urethra. Each panel shows sections stained with H and E. [A] shows longitudinal sections of the urethra illustrating (a) the bladder neck and proximal urethra and (b) the mid and distal urethra. [B] shows transverse sections taken from different positions along the urethra; (a), bladder neck (b), proximal urethra (c), mid urethra (d), distal urethra and (e) external urethral meatus. The dorsal aspect of the urethra are marked (D). Individual features are identified: lumen (lum), epithelium (epi), smooth muscle (sm), striated muscle sphincter (ss), detrusor (det), epithelial folds (F) and blood vessels (bv). Scale bars in each panel are 800μm.

118x82mm (300 x 300 DPI)

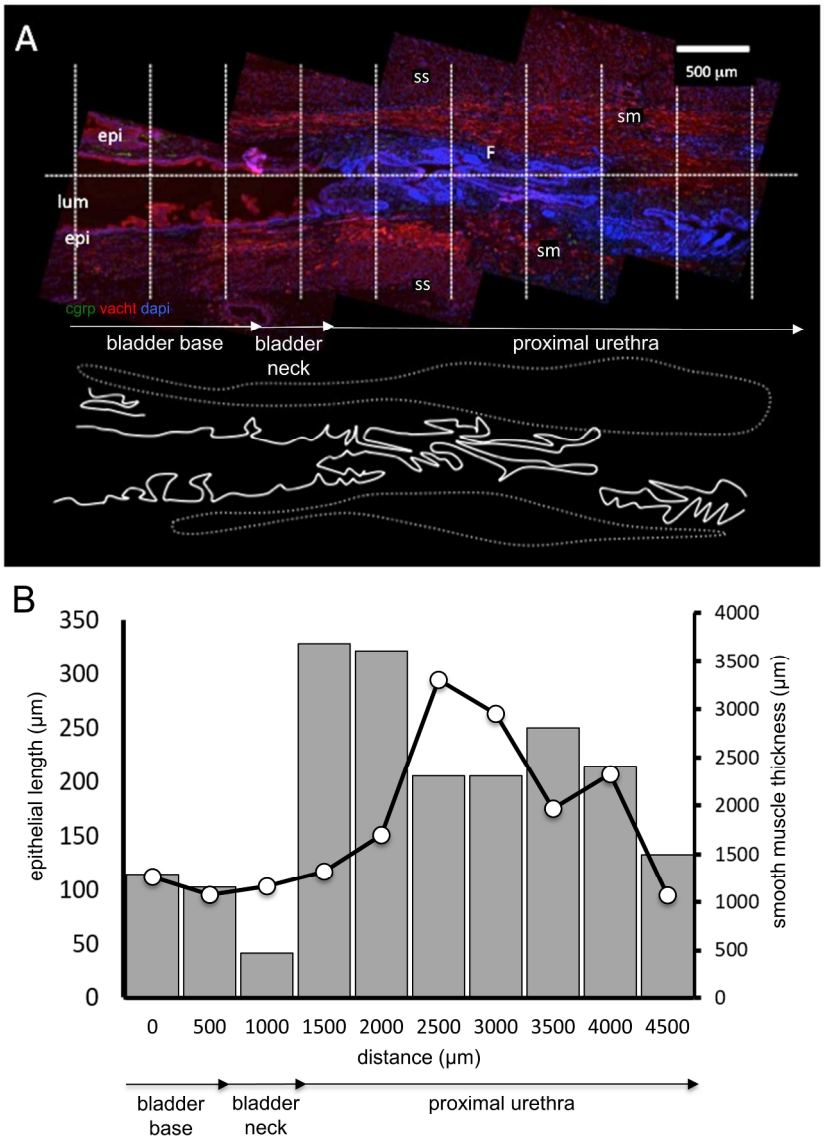

Fig. 2. Illustration of urethral folding in the bladder neck/proximal urethra and the position of the muscle sphincters. [A] the upper panel is a montage of images illustrating the bladder neck and proximal urethra over a distance of 5 mm (vertical lines are 500 µm apart). It shows immunofluorescent images illustrating staining for cgrp (green), vacht (red) and the nuclear stain dapi (blue). The lumen (lum), epithelium (epi), smooth muscle internal sphincter (sm) and striated muscle sphincter (ss) are indicated. The region of high folding is also shown (F). The lower section is a tracing of the features in the upper panel drawn for clarity, showing the epithelium (solid line) and the internal sphincter (dotted line). [B] illustrates an analysis of this section depicting the total length of epithelium within successive 500 µm wide regions along the urethra (grey histograms). The thickness of the smooth muscle layer is also shown for the corresponding 500 µm intervals along the urethra (o). Note that the point of maximum muscle thickness is distal to the point of maximal urethral folding. Similar data showing such a displacement between the position of maximum folding and maximum smooth muscle thickness were seen in all urethras studied (n=5).

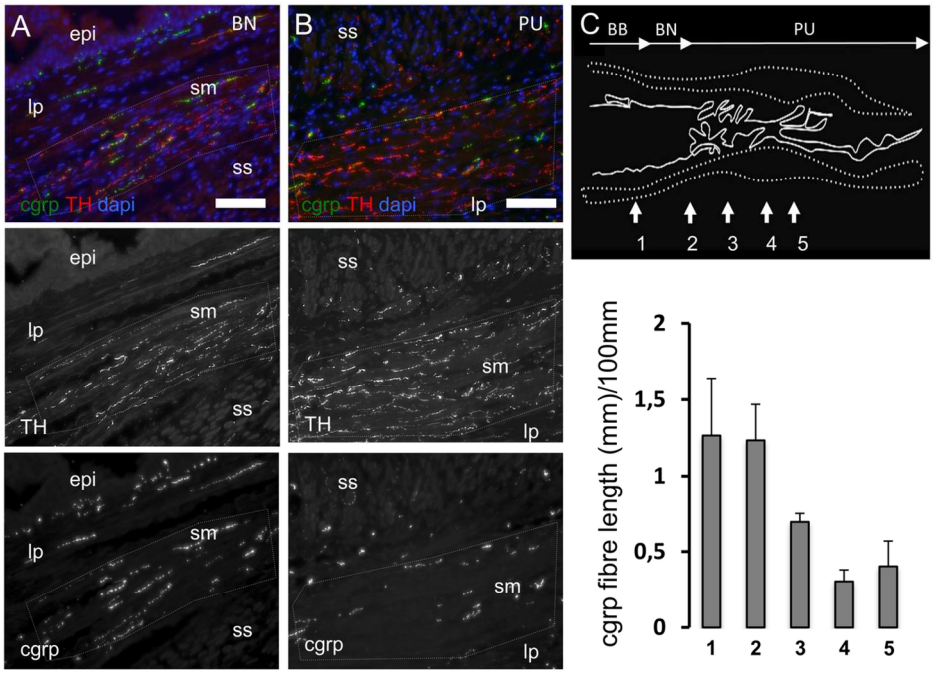

Fig. 3. Illustration of the putative sensory innervation of the smooth muscle in the bladder neck and proximal urethra. Smooth muscle is illustrated in the bladder neck [A] and proximal urethra [B]. The sections are stained for the nerve markers TH (red), cgrp (green) and the nuclear marker dapi (blue). The upper panels show the combined images while the middle and lower show the composite TH and cgrp images. The epithelium (epi), lamina propria (lp), smooth muscle (sm) and striated muscle sphincter (ss) are indicated. Regions of the smooth muscle are identified (dotted lines) for nerve profile analysis. Note the near absence of cgrp-IR fibres in the smooth muscle of the proximal urethra. Calibration bars in [A] and [B] are 150 µm. [C] shows a more detailed analysis of the distribution of cgrp-IR fibres. The upper panel identifies 5 arbitrary regions (1-5) in the bladder base (BB), bladder neck (BN) and proximal urethra (PU). Section [A] corresponds with arbitrary region 2 and section [B] corresponds with arbitrary region 4. In each of the arbitrary regions (1-5) the extent of cgrp innervation was determined in representative area by determining fibre length per area. Values are mean + standard deviation (n=5) for representative areas. Note the clear reduction in cgrp innervation in the smooth muscle of the proximal urethra.

121x88mm (300 x 300 DPI)

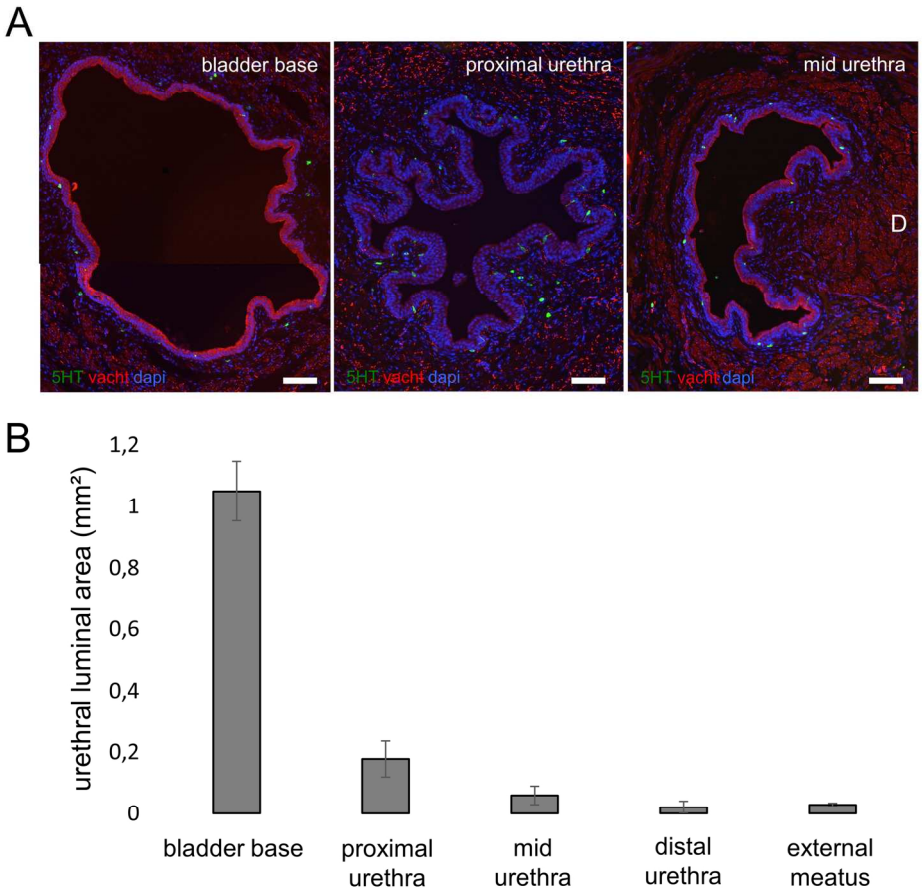

Fig. 4. Cross sections of the bladder base, proximal and mid urethra. [A] illustrates 3 transverse sections stained for the neuronal markers 5HT (green), vacht (red) and the nuclear marker dapi (blue). The left panel shows the large lumen diameter of the bladder base. The middle panel shows the high degree of epithelial folding in the proximal urethra. The right panel illustrates a thickening of the smooth muscle in the mid urethra. Note that, in this region, this is on the dorsal side (D) of the urethra and protrudes into the lumen, coming into close proximity with the ventral surface. Calibration bars in [A], [B] and [C] are 200 µm. [B] illustrates an analysis of the lumen dimensions at different locations along the urethra. In order to take into account the folding of the urethral wall, measurements were made of the lumen cross-sectional area. Data are mean values + standard deviation (n=7).

159x145mm (300 x 300 DPI)

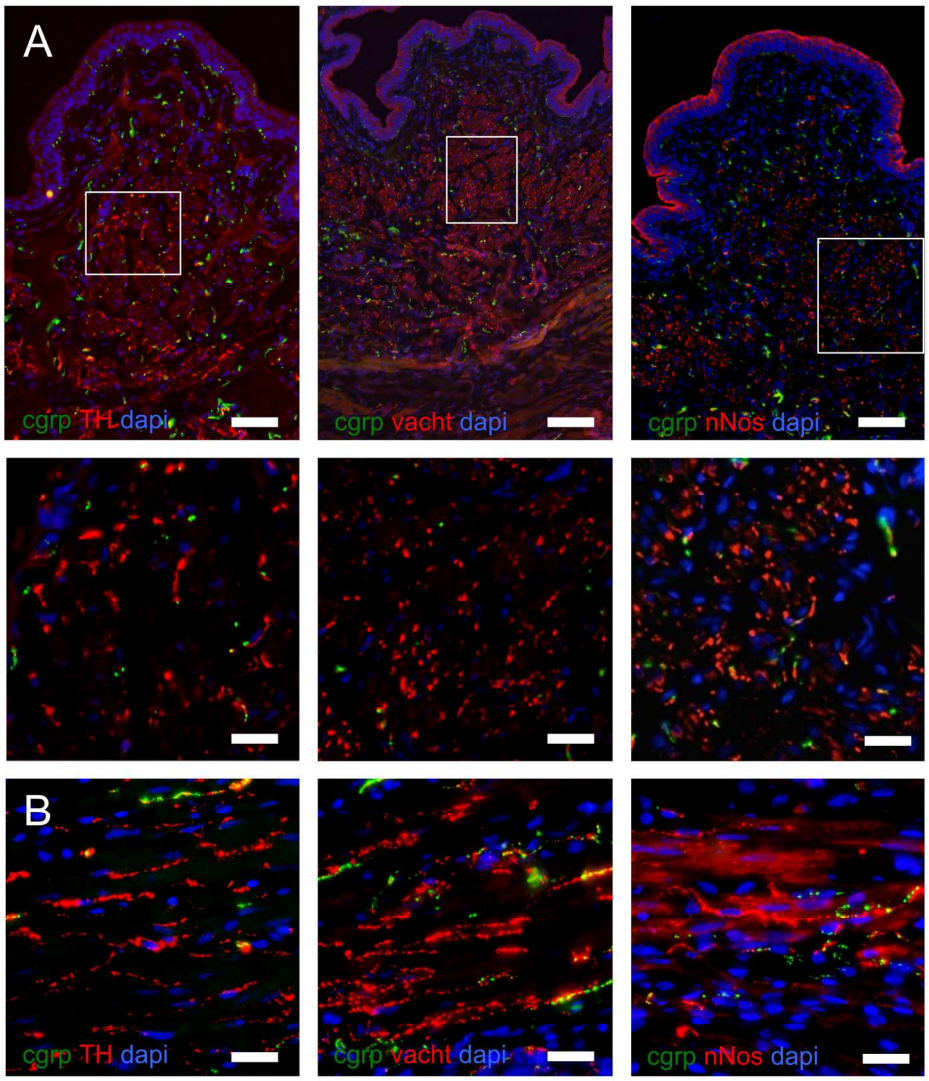

Fig. 5. Illustration of the innervation of the luminal protrusion on the dorsal side of the mid urethra. [A] shows low power transverse sections of the thickening in the mid urethra stained (from left to right) for TH (red) and cgrp (green); vacht (red) and cgrp (green); nNos (red) and cgrp (green). All sections are also stained for dapi (blue). The middle panels shows higher resolution images of [A] (boxes) illustrating distinct TH, vacht and nNos-IR nerve fibres as well as cgrp-IR fibres. Note the orientation of the fibres that appears as 'dots' or short structures. [B] shows images from a different urethra illustrating the innervation in the same mid-urethral region with the same stainings. In this preparation the tissue was cut longitudinally. Note that here the fibres appear long suggesting that they run predominantly parallel to the long axis of the tissue. Calibration bars: [A], 200 µm; middle panels, 20 µm; [B], 20 µm.

187x218mm (300 x 300 DPI)

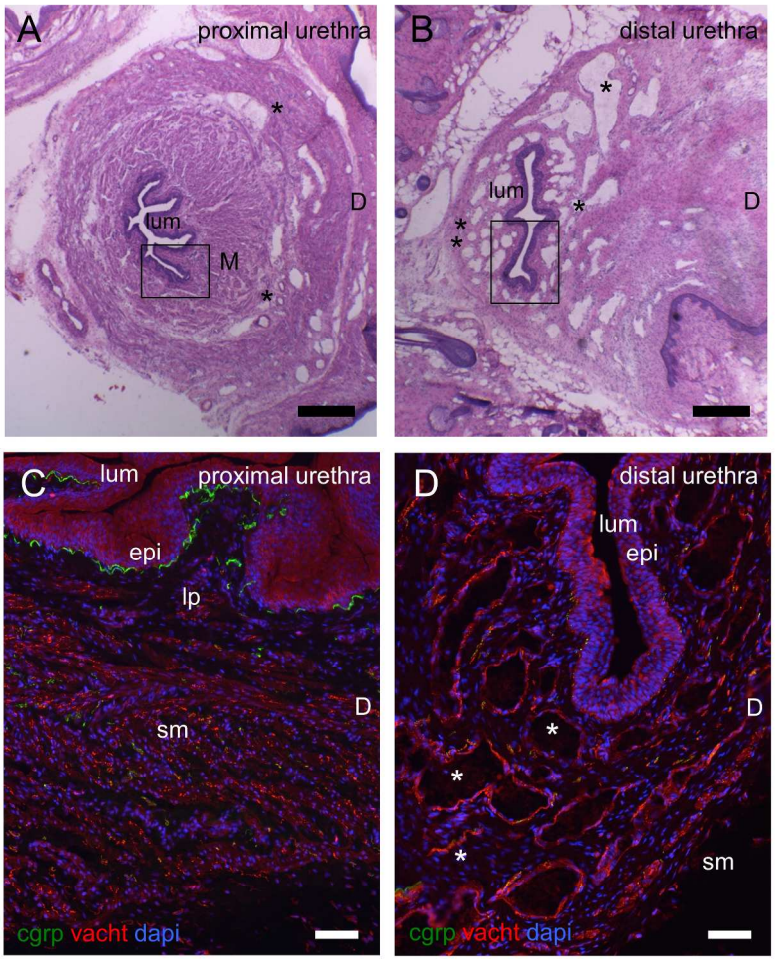

Fig. 6. The distribution of large blood vessels in the proximal and distal urethra. [A] and [B] show respectively transverse H and E sections of the proximal urethra and distal urethra. In each panel examples of vessels are indicated (*). Note that in the proximal urethra the vessels are located primarily between the major muscle mass (M) and the fascia of the dorsal margin (D). In the distal urethra, a region of dense vessels is seen close to the lumen (lum). [C] and [D] show sections of the proximal and distal urethra respectively stained for the nerve markers cgrp (green) and vacht (red). Sections are also stained for the nuclear marker dapi (blue). Note, in the proximal urethra, the presence of cgrp-IR fibres close to the epithelium (epi) but not in the smooth muscle layer (sm). In the distal urethra, vacht-IR fibres are seen in close proximity to the vessels. Calibration bars: [A]/[B] 800µm and [C]/[D] 200 µm. lp = lamina propria.

229x303mm (300 x 300 DPI)

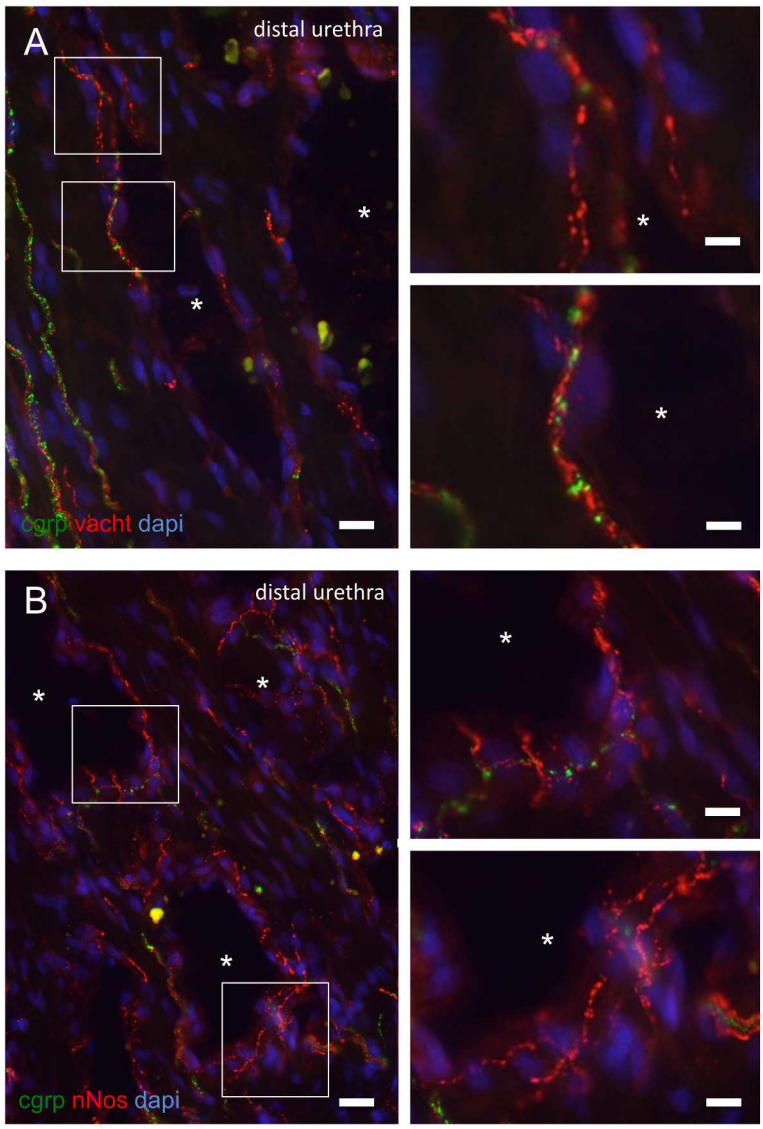

Fig. 7. High resolution images illustrating the innervation of the blood vessels in the distal urethra. [A] shows a section stained for the nerve markers vacht (red) and cgrp (green). All sections are also stained for the nuclear marker dapi (blue). The left panel shows a low power image while the right panels show the identified regions (boxes) at higher magnification. Vessel lumens are indicated (*). Arrows point to distinct vacht-IR and cgrp-IR fibres in the wall of the vessels. [B] shows sections stained for nNos (red), cgrp (green) and dapi (blue). Vessel lumen are indicated (*) and arrows point to distinct nNos-IR nerves. The panels on the right show the identified regions (boxes) of the image on the left at higher magnification. nNos-IR nerves are clearly seen in the vessel wall. Calibration bars in [A] and [B] large panels are 15 µm and side panels are 6 µm.

229x303mm (300 x 300 DPI)

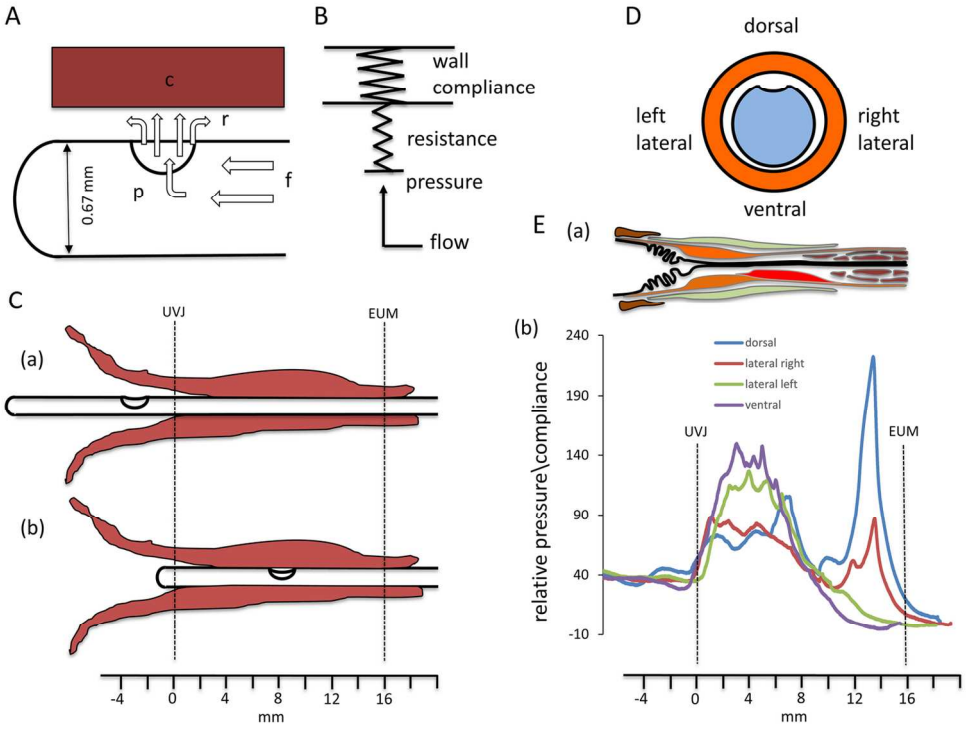

Fig. 8. Estimation of urethral wall compliance along its length and on different axes [A] illustrates the aperture of the closed ended catheter (catheter diameter 0.67 mm, aperture diameter 0.2 mm). Saline is forced through the opening at a rate of 0.3 ml/min (direction of flow (f) illustrated by arrows) resulting in a basal catheter pressure (p). When the catheter opening is brought close to the urethral wall the resistance to flow (r) increases and the pressure rises. If the urethral wall over the aperture is passive and elastic (high compliance (c)) then the wall will contribute only a small amount to the resistance and the catheter pressure will remain close to basal pressure. However, if the wall is stiff (low compliance), the fluid flow will not displace the wall and the resistance to flow will be greater. As a result, the pressure in the catheter will rise. The catheter pressure is therefore, in part, related to the compliance of the underlying urethral wall. [B] illustrates a simple representation of the elements of the system. [C] illustrates the catheter with the aperture in the bladder lumen (a) and as it is pulled through the urethra (b). The dotted lines are assumed to represent the urethrovesical junction (UVJ) and the external urethral meatus (EUM). [D] illustrates the position of the aperture in relation to the urethral wall. The aperture can be rotated to estimate the wall compliance in the dorsal and ventral aspects and also in the lateral walls. [E] (b) illustrates 4 sample records of catheter pressure from one animal (supine position) as the catheter is pulled from the bladder through the urethra (10mm/min). The different traces were made with the aperture pointing to the dorsal, ventral, left lateral and right lateral wall. A reference point to identify the position of the aperture was determined by the position of first pressure inflection during a withdrawal (0mm). Negative values represent positions where the aperture is in the bladder and positive values at different positions along the urethra. The cartoon summarizing the morphological features along the urethra is also shown (a) in an attempt to relate structures to the pressure/compliance changes (see legend Fig. 9 for details).

68x51mm (600 x 600 DPI)

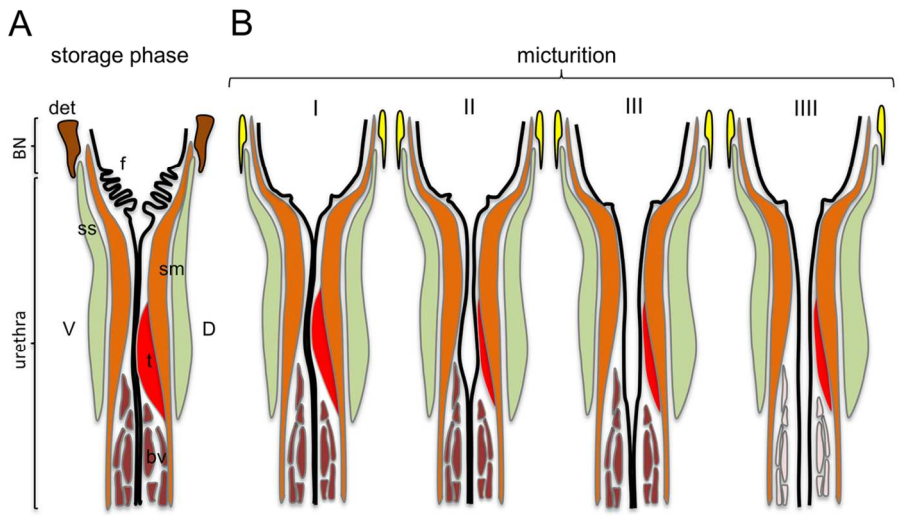

Fig. 9. Cartoons summarizing the major structural elements observed in the female rat urethra. [A] shows the major elements: detrusor (det), folded epithelium of the proximal urethra (f), striated muscle sphincter (ss), smooth muscle (sm), mid urethral smooth muscle thickening (t) and distal urethral blood vessels (bv). The bladder neck (BN), the urethra, ventral (V) and distal (D) positions are shown. Panel A also illustrates a possible arrangement where all of the different elements are in place to produce a closed urethra, i.e. as during the filling or storage phase. [B] illustrates how each of the component systems might change to lead to an opening of the urethral lumen: (I) opening of the bladder neck and unfolding of the proximal epithelial folds, (II)/(III) opening urethral lumen by relaxation of urethral smooth and striated muscle, and (IIII) opening distal urethral lumen by overcoming of vesical resistance.

57x31mm (600 x 600 DPI)